HHS Public Access

Author manuscript

J Urol. Author manuscript; available in PMC 2016 January 26.

Published in final edited form as:

J Urol. 2015 August ; 194(2): 364–370. doi:10.1016/j.juro.2015.02.080.

Image Guided Focal Therapy of Magnetic Resonance Imaging Visible Prostate Cancer: Defining a 3-Dimensional Treatment Margin Based on Magnetic Resonance Imaging-Histology Co-Registration Analysis

Julien Le Nobin[*], **Andrew B. Rosenkrantz**, **Arnauld Villers**, **Clément Orczyk**, **Fang-Ming Deng**, **Jonathan Melamed**, **Artem Mikheev**, **Henry Rusinek**, and **Samir S. Taneja**[†]

Division of Urologic Oncology, Department of Urology (JLN, CO, SST), and Departments of Radiology (ABR, AM, HR) and Pathology (FMD, JM), New York University Langone Medical Center, New York, New York, and Departments of Urology, University Hospital of Lille (JLN, AV), Lille and Unités Mixtes de Recherche 6301-CERVOxy Group, University Hospital of Caen, Caen, France

Abstract

Purpose—We compared prostate tumor boundaries on magnetic resonance imaging and radical prostatectomy histological assessment using detailed software assisted co-registration to define an optimal treatment margin for achieving complete tumor destruction during image guided focal ablation.

Materials and Methods—Included in study were 33 patients who underwent 3 Tesla magnetic resonance imaging before radical prostatectomy. A radiologist traced lesion borders on magnetic resonance imaging and assigned a suspicion score of 2 to 5. Three-dimensional reconstructions were created from high resolution digitalized slides of radical prostatectomy specimens and co-registered to imaging using advanced software. Tumors were compared between histology and imaging by the Hausdorff distance and stratified by the magnetic resonance imaging suspicion score, Gleason score and lesion diameter. Cylindrical volume estimates of treatment effects were used to define the optimal treatment margin.

Results—Three-dimensional software based registration with magnetic resonance imaging was done in 46 histologically confirmed cancers. Imaging underestimated tumor size with a maximal discrepancy between imaging and histological boundaries for a given tumor of an average ± SD of 1.99 ± 3.1 mm, representing 18.5% of the diameter on imaging. Boundary underestimation was larger for lesions with an imaging suspicion score 4 or greater (mean 3.49 ± 2.1 mm, $p < 0.001$) and a Gleason score of 7 or greater (mean 2.48 ± 2.8 mm, $p = 0.035$). A simulated cylindrical treatment volume based on the imaging boundary missed an average 14.8% of tumor volume compared to that based on the histological boundary. A simulated treatment volume based on a 9 mm treatment margin achieved complete histological tumor destruction in 100% of patients.

[*]Correspondence: Department of Urology, Hôpital Claude Huriez, Hospitalier Régional Universitaire de Lille, 1, place de Verdin, 59037 Lille Cedex, France (telephone: +33 659 512 377; FAX: +33 320 446 915; julien.lenobin@gmail.com).

[†]Financial interest and/or other relationship with Hitachi-Aloka, Biobot, Healthtronics, Elsevier and Trod.

Conclusions—Magnetic resonance imaging underestimates histologically determined tumor boundaries, especially for lesions with a high imaging suspicion score and a high Gleason score. A 9 mm treatment margin around a lesion visible on magnetic resonance imaging would consistently ensure treatment of the entire histological tumor volume during focal ablative therapy.

Keywords

prostatic neoplasms; magnetic resonance imaging; image processing; computer-assisted; pathology; risk

Focal therapy is gaining increasing interest as primary treatment for prostate cancer.[1] This trend is partly driven by growing awareness of the indolent nature and excellent survival rate of most newly diagnosed lesions such that radical prostatectomy and radiation therapy with their associated impact on quality of life may not be warranted.[2] Although active surveillance provides a reasonable alternative in many patients with low risk tumors, this approach has limitations, including the intensity of followup evaluation to which patients are subjected and the associated anxiety of potentially missing the window of opportunity for cure.[3]

While ablative therapy for prostate cancer historically entailed total, subtotal or hemitotal ablation, more recent reports describe truly focal ablation procedures targeting the expected location of dominant tumors.[4,5] This approach is supported by the emergence of newer ablation technologies, including laser based thermotherapy,[4,6] focal cryoablation[7] or photodynamic therapy,[8] which allow for more precise definition of tissue destruction margins. Thus, such procedures require a method to anticipate tumor margins and thereby guide decisions on the boundary of the ablated region to avoid under treatment.

The ability to precisely define focal lesion volume by MRI would have immense value for guiding focal ablative therapy.[9] Past studies compared tumor volumes between MRI and histopathology assessment.[10–13] Using affine transformation and compensation for changes in volume and shape[14] we previously performed such an investigation with a validated, automated 3D co-registration system.[15] We observed consistent underestimation of tumor volume by MRI, indicating that actual tumor boundaries are expected to be located beyond the boundaries predicted by the visualized lesion on MRI. This difference in lesion boundaries has a critical impact in planning and performing focal therapy procedures, given that treatment of only the MRI visualized lesion leaves a portion of tumor untreated due to the larger histological volume. Therefore, a method is needed to define a target volume for focal therapy of an MRI visualized lesion to reliably treat the entire tumor volume. Such a methodology would be important to achieve optimal oncologic control using emerging MRI targeted focal therapeutic procedures.

Thus, in the current study we compared the boundaries of prostate tumors between MRI and histopathology evaluation using co-registration software to define an optimal treatment margin and achieve complete tumor destruction at image guided focal ablation.

MATERIALS AND METHODS

Study Population

This retrospectively study was approved by our institutional review board. A waiver of written informed consent was granted. We initially identified 37 patients who underwent MRI at our center before prostatectomy. In these patients a dominant tumor was identified on histopathology assessment and visualized on MRI. This cohort was evaluated in a prior study comparing tumor volumes on MRI and radical prostatectomy pathological assessment.[15] Four of the 37 patients were excluded from analysis because of tumor volume greater than 3 cc on preoperative MRI since patients with a lesion of this size would not be selected for focal therapy. Thus, the final cohort comprised 33 patients with a mean ± SD age of 60.7 ± 5.4 years. Median preoperative PSA was 4.8 ng/ml (range 0.32 to 19.5), including 27 patients with PSA less than 10 ng/ml, 4 with PSA 10 to 15 ng/ml and 2 with PSA greater than 15 ng/ml.

MRI Data Acquisition

MRI was performed using a 3 Tesla whole body system and a pelvic phased array coil. Sequences included multiplanar T2WI and axial diffusion-weighted imaging of the prostate (b-values 50 and 1,000 seconds per mm^2) with apparent diffusion coefficient reconstruction. Dynamic contrast enhanced imaging of the prostate was done with 0.1 mmol/kg gadolinium chelate and 5.5-second temporal resolution.

Histopathology Analysis

A standard Stanford protocol was used for pathological assessment as previously described in detail.[15,16] Photographs were taken of intact slices using a digital camera before further processing. Subsequent histological slides underwent high resolution digitalization at 400× magnification using a Leica SN400 (Leica Microsystems, Wetzlar, Germany). Digital images were combined with Photoshop® to form virtual whole mount images using the photographs of intact slices for guidance. A single uropathologist marked tumor borders and recorded the GS of each lesion. Tumors were stratified into a low grade group (GS 6) and a high grade group (GS 7 or greater).

MRI Assessment and Histopathology Co-Registration

For each patient a genitourinary radiologist traced the boundary of the dominant lesion on each slice on which the lesion was visible. This was performed using only T2WI in the peripheral and transition zones. The radiologist was aware of the general location of the dominant lesion from the histopathology assessment but not of the precise tumor boundaries. A score was assigned to each lesion on a Likert scale of 1 to 5 to indicate the likelihood of clinically significant cancer.[17] These scores were considered low suspicion—3 or less, or high suspicion—4 or greater.

Software was used to perform co-registration between MRI and digital 3D surgical specimens constructed from the photographs of gross slices. The 3D specimen was initially reconstructed with Image J®, version 1.44e (http://imagej.nih.gov/ij/) and Photoshop.

Subsequent co-registration with MRI was done using in-house Fire-Voxel software (https://files.nyu.edu/hr18/public/).

Focal Therapy Treatment Volume Simulation

Two ROIs were placed for each tumor. One ROI corresponded to the lesion traced on T2WI and the other corresponded to the lesion on the 3D histological data set after co-registration with T2WI (registered histology). To compare tumor boundaries between T2WI and registered histology the software was first used to calculate the HD between the 2 ROIs for each individual slice. HD provides a single value representing the distance between the set of points represented by each ROI.[18,19] A mean and a maximum HD were calculated, corresponding to the mean and maximum HD across all slices comprising the tumor (fig. 1). Each HD is reported in mm and the percent of the lesion maximum diameter on T2WI. The largest attainable HD on any MRI slice comprising tumor is defined as the tumor Hausdorff Max. Finally, for each tumor 2 cylinders centered around the lesion on T2WI were constructed to simulate potential focal therapy treatment zones. One cylinder was MCyl, of which the diameter corresponded to the maximal lesion diameter on T2WI, and the other was HCyl, of which the diameter corresponded to the summation of the maximal lesion diameter on T2WI and the maximum HD. Using this approach MCyl encompassed the entire lesion on T2WI and HCyl encompassed the entire co-registered histological lesion. Figure 2 shows focal therapy simulations using these theoretical cylinders to define the treatment zone. Subsequently the software was used to calculate the tumor volume that would be untreated when targeting MCyl as well as the volume of benign tissue treated when targeting HCyl.

Statistical Analysis

For each tumor the mean and maximum HD were compared. HD was stratified based on imaging and histological characteristics, including GS, tumor size and MRI SS. The various volume assessments were compared using the paired t-test and Wilcoxon test for data with normal and nonnormal distributions, respectively, with significance considered at $p = 0.05$. SPSS®, version 14.0 was used for analysis.

RESULTS

Lesion Characteristics

A total of 46 tumors were visualized in the 33 study patients, including 37 (80.4%) in the peripheral zone and 9 (19.6%) in the transition zone. On histological assessment GS was 6 in 10 lesions (21.7%), 7 in 35 (76.1%), including Gleason 3 + 4 in 26 and 4 + 3 in 9, and 9 in 1 (2.2%). MRI SS was categorized as low in 14 lesions (30.4%) and as high in 32 (69.6%). On T2WI mean tumor volume was 0.71 ± 0.51 cc and mean maximal diameter was 12.5 ± 3.29 mm. On registered histology mean tumor volume was 1.05 ± 0.79 cc and mean maximal diameter was 14.9 ± 5.14 mm. Table 1 lists characteristics.

Tumor Boundary Assessment

In general MRI substantially underestimated tumor size. Accordingly in all lesions mean HD was 0.50 ± 0.86 mm and mean maximum HD was 1.99 ± 3.1 mm. Maximum HD was

significantly greater for high suspicion lesions and for high grade lesions (p = 0.002 and 0.035, respectively, table 2). Figure 3 shows maximum HD values stratified by tumor characteristics.

Treatment Margin

Figure 4 shows tumor diameter on T2WI compared to maximum HD, corresponding to the hypothetical margin of the histological lesion around the MRI lesion. This mean hypothetical histological tumor margin was 18.5% of MRI tumor diameter (95% CI −32.1 to 69.2). A total of 12 (26.1%), 25 (54.3%), 34 (73.9%), 43 (93.5%) and 46 tumors (100%) were located within the 1, 3, 5, 7 and 9 mm simulated treatment margins, respectively. Thus, all lesions were fully treated within the 9 mm curve regardless of lesion MRI diameter, MRI SS or GS.

Cylinder Volume and Missed Tumors

Table 3 lists focal treatment effect volumetric simulations performed using 3D cylinder volumes. For all lesions MCyl had a mean volume of 2.38 cc, representing 5.3% of prostate volume. It missed an average of 0.16 cc tumor volume (14.8%). HCyl had a mean volume of 4.32 cc, representing 10% of prostate volume. It was estimated to treat 100% of tumor volume.

DISCUSSION

In a previous series we used 3D digital co-registration software to determine that MRI substantially underestimates prostatic tumor volume and the underestimation was more marked for high GS and high suspicion lesions.[15] These findings have key implications for image guided focal therapy. Focally ablative treatment entails destruction of the tumor and a rim of benign tissue.[20] Therefore, it is important to estimate tumor margins to guide ablation. Our results suggest that a much larger prostate region than that directly visualized on MRI warrants ablation to be confident of full tumor destruction. Specifically our findings suggest that a treatment zone approximately 20% larger than the apparent tumor on MRI would ensure treatment of the full tumor in more than 95% of cases. In addition, a 9 mm margin would ensure treatment of the tumor in all cases.

The discrepancy in MRI and histology boundaries is most relevant at the lesion noncapsular margin, given the tendency for tumors to originate close to the capsule and show centripetal growth in the gland.[21] Because extraprostatic extension in patients who undergo radical prostatectomy generally resides within 3 mm of the capsule,[22] based on our data we suggest that image guided focal ablation may be optimally performed with a combination of a 9 mm noncapsular and a 3 mm capsular treatment margin to balance complete tumor destruction and healthy tissue preservation. Despite our choice of a cylindrical ablation volume we believe that our findings apply broadly to any form of focal therapy. Since the maximal tumor diameter used in our size calculation resided in the center of the cylinder, our findings would theoretically be applicable even in the setting of a fusiform or spherical ablation zone.

Past studies of various forms of focal therapy of prostate cancer provide results on cancer control based on posttreatment biopsies treatment. However, only a few of these studies

provide details on the safety margin required during the procedure. A review of these studies suggested that approximately 20% of patients may have positive biopsies after focal treatments, although often with low grade, low volume disease. For example, a group reported that 6 months after photodynamic therapy around 20% of patients had a positive biopsy.[8] In another study of cryotherapy biopsies were positive at 1 year in 19% of patients, of whom all had GS 3 + 3 = 6 in 1 or 2 cores.[23] In contrast to our findings, another past study demonstrated that on the noncapsular border the median distance between the imaging and histopathology boundaries was only 1.4 mm (range 0 to 12).[24] In that study expanding the treatment zone by 5 mm at the noncapsular margin allowed inclusion of 95% of the tumor volume not initially within the MRI contour. However, our results indicate more pronounced underestimation of MRI volume. We observed that a 5 mm margin would cover only 74% of the tumor and a 9 mm margin was needed to cover 100%. While the explanation of such differences in results is uncertain, our use of 3D co-registration technology to improve reconstruction of the tumor histological shape and its correlation with MRI that suggests caution is warranted if applying the shorter treatment margins suggested in the previous literature.

We evaluated individual lesions using an institutionally refined Likert scale of 1 to 5. We have considerable experience with the scale and previously found that it has diagnostic accuracy similar to that of the ESUR PI-RADS (European Society of Urogenital Radiology Prostate Imaging Reporting and Data System) scoring scheme in the peripheral zone and somewhat better accuracy in the transition zone.[25] Given the propensity of MRI to underestimate the size of intermediate and high risks tumors, caution should be exerted when selecting these men for focal ablation.

Our study did not define the nature of tumor borders not visualized on MRI when planning focal therapy. Within the context of individual tumors we previously found that those detected by MRI are morphologically distinct from those that are not detected.[26] While undetected lesions are typically of lower grade and more sparse, to our knowledge the clinical significance in regard to the risk of recurrence and progression is unknown. Future studies of solid vs sparse growth patterns of portions of the tumors not visualized on MRI may help account for the underestimation of tumor volume observed in this series.[27]

Our study has a number of limitations. 1) While our virtual whole mount methodology was not previously tested for tumor location accuracy, we believe that our co-registration methodology, which accounts for gland deformation and shrinkage in the specimen, remains a strength of our study. 2) Tumor boundaries were assessed only on T2WI but a prior study showed greater underestimation of tumor volume using diffusion-weighted imaging and T2WI.[15] Thus, we believe that T2WI may be the most common sequence used to guide focal ablation. 3) The radiologist was aware of the general location of tumors on histopathology but not of the borders when tracing tumor boundaries on MRI. While this unblinded design precluded an assessment of the reader accuracy of tumor localization, the approach made it easier to ensure that boundaries were compared between matching lesions on MRI and histology. 4) Tumor 3D morphology varied among patients and could not be adequately accounted for due to our sample size. 5) Our findings were derived from

computer based simulations. Prospective clinical studies are required to validate our estimations in patients undergoing focal ablative therapy.

CONCLUSIONS

MRI underestimated the boundaries of prostate tumors, particularly the boundaries of high suspicion and high grade lesions. Based on simulations using co-registration software we found that a 9 mm treatment margin around the MRI target consistently ensured treatment of the entire histological tumor volume. This proposed 9 mm treatment margin would be optimally applied to the non-capsular margin of the lesion due to the shorter degree of tumor extension expected along the lesion capsular margin. Such insights should be considered during the planning of focal ablation targeting MRI lesions.

Acknowledgments

Supported by the Joseph and Diane Steinberg Charitable Trust, an Association Française d'Urologie (bourse de l'AFU 2012) grant, National Center for Research Resources, National Institutes of Health Grant 1UL1RR029893, Cancer Center Support Grant P30CA016087 (Histopathology Core, Laura and Isaac Perlmutter Cancer Center) and National Center for Advancing Translational Sciences, National Institutes of Health Grant UL1 TR00038.

Abbreviations and Acronyms

3D	3-dimensional
GS	Gleason score
HCyl	histological cylinder
HD	Hausdorff distance
Hausdorff Max	Hausdorff maximum principle
MCyl	MRI cylinder
MRI	magnetic resonance imaging
ROI	region of interest
SS	suspicion score
T2WI	T2-weighted imaging

References

1. Valerio M, Ahmed HU, Emberton M, et al. the role of focal therapy in the management of localised prostate cancer: a systematic review. Eur Urol. 2014; 66:732. [PubMed: 23769825]
2. Parker C, Muston D, Melia J, et al. A model of the natural history of screen-detected prostate cancer, and the effect of radical treatment on overall survival. Br J Cancer. 2006; 94:1361. [PubMed: 16641912]
3. Klotz L, Zhang L, Lam A, et al. Clinical results of long-term follow-up of a large, active surveillance cohort with localized prostate cancer. J Clin Oncol. 2010; 28:126. [PubMed: 19917860]
4. Oto A, Sethi I, Karczmar G, et al. MR imaging-guided focal laser ablation for prostate cancer: phase I trial. Radiology. 2013; 267:932. [PubMed: 23440319]

5. Ahmed HU, Hindley RG, Dickinson L, et al. Focal therapy for localised unifocal and multifocal prostate cancer: a prospective development study. Lancet Oncol. 2012; 13:622. [PubMed: 22512844]
6. Colin P, Mordon S, Nevoux P, et al. Focal laser ablation of prostate cancer: definition, needs, and future. Adv Urol. 2012; 2012:589160. [PubMed: 22666240]
7. Bomers JGR, Yakar D, Overduin CG, et al. MR imaging-guided focal cryoablation in patients with recurrent prostate cancer. Radiology. 2013; 268:451. [PubMed: 23525206]
8. Azzouzi A-R, Barret E, Moore CM, et al. TOOKAD(®) Soluble vascular-targeted photodynamic (VTP) therapy: determination of optimal treatment conditions and assessment of effects in patients with localised prostate cancer. BJU Int. 2013; 112:766. [PubMed: 24028764]
9. Hoeks CMA, Barentsz JO, Hambrock T, et al. Prostate cancer: multiparametric MR imaging for detection, localization, and staging. Radiology. 2011; 261:46. [PubMed: 21931141]
10. Nakashima J, Tanimoto A, Imai Y, et al. Endorectal MRI for prediction of tumor site, tumor size, and local extension of prostate cancer. Urology. 2004; 64:101. [PubMed: 15245944]
11. Ponchietti R, Di Loro F, Fanfani A, et al. Estimation of prostate cancer volume by endorectal coil magnetic resonance imaging vs. pathologic volume. Eur Urol. 1999; 35:32. [PubMed: 9933792]
12. Coakley FV, Kurhanewicz J, Lu Y, et al. Prostate cancer tumor volume: measurement with endorectal MR and MR spectroscopic imaging. Radiology. 2002; 223:91. [PubMed: 11930052]
13. Kirkham APS, Emberton M, Allen C. How good is MRI at detecting and characterising cancer within the prostate? Eur Urol. 2006; 50:1163. [PubMed: 16842903]
14. Orczyk C, Rusinek H, Rosenkrantz AB, et al. Preliminary experience with a novel method of three-dimensional co-registration of prostate cancer digital histology and in vivo multi-parametric MRI. Clin Radiol. 2013; 68:e652. [PubMed: 23993149]
15. Le Nobin J, Orczyk C, Deng FM, et al. Prostate tumor volumes: agreement between MRI and histology using novel co-registration software. BJU Int. 2014; 114:e105. [PubMed: 24673731]
16. McNeal JE, Bostwick DG, Kindrachuk RA, et al. Patterns of progression in prostate cancer. Lancet. 1986; 1:60. [PubMed: 2867314]
17. Barentsz JO, Richenberg J, Clements R, et al. ESUR prostate MR guidelines 2012. Eur Radiol. 2012; 22:746. [PubMed: 22322308]
18. Morain-Nicolier F, Lebonvallet S, Baudrier E, et al. Hausdorff distance based 3D quantification of brain tumor evolution from MRI images. Conf Proc IEEE Eng Med Biol Soc. 2007; 2007:5597. [PubMed: 18003281]
19. Sim DG, Kwon OK, Park RH. Object matching algorithms using robust Hausdorff distance measures. IEEE Trans Image Process. 1999; 8:425. [PubMed: 18262885]
20. Lindner U, Lawrentschuk N, Trachtenberg J. Image guidance for focal therapy of prostate cancer. World J Urol. 2010; 28:727. [PubMed: 20963422]
21. McNeal JE, Haillot O. Patterns of spread of adenocarcinoma in the prostate as related to cancer volume. Prostate. 2001; 49:48. [PubMed: 11550210]
22. Ball MW, Partin AW, Epstein JI. Extent of extraprostatic extension independently influences biochemical recurrence-free survival: evidence for further pT3 subclassification. Urology. 2015; 85:161. [PubMed: 25440818]
23. Barqawi AB, Stoimenova D, Krughoff K, et al. Targeted focal therapy in the management of organ confined prostate cancer. J Urol. 2014; 192:749. [PubMed: 24641910]
24. Anwar M, Westphalen AC, Jung AJ, et al. Role of endorectal MR imaging and MR spectroscopic imaging in defining treatable intraprostatic tumor foci in prostate cancer: quantitative analysis of imaging contour compared to whole-mount histopathology. Radiother Oncol. 2014; 110:303. [PubMed: 24444524]
25. Rosenkrantz AB, Kim S, Lim RP, et al. Prostate cancer localization using multiparametric MR imaging: comparison of Prostate Imaging Reporting and Data System (PI-RADS) and Likert scales. Radiology. 2013; 269:482. [PubMed: 23788719]
26. Rosenkrantz AB, Mendrinos S, Babb JS, et al. Prostate cancer foci detected on multiparametric magnetic resonance imaging are histologically distinct from those not detected. J Urol. 2012; 187:2032. [PubMed: 22498205]

27. Langer DL, van der Kwast TH, Evans AJ, et al. Intermixed normal tissue within prostate cancer: effect on MR imaging measurements of apparent diffusion coefficient and T2–sparse versus dense cancers. Radiology. 2008; 249:900. [PubMed: 19011187]

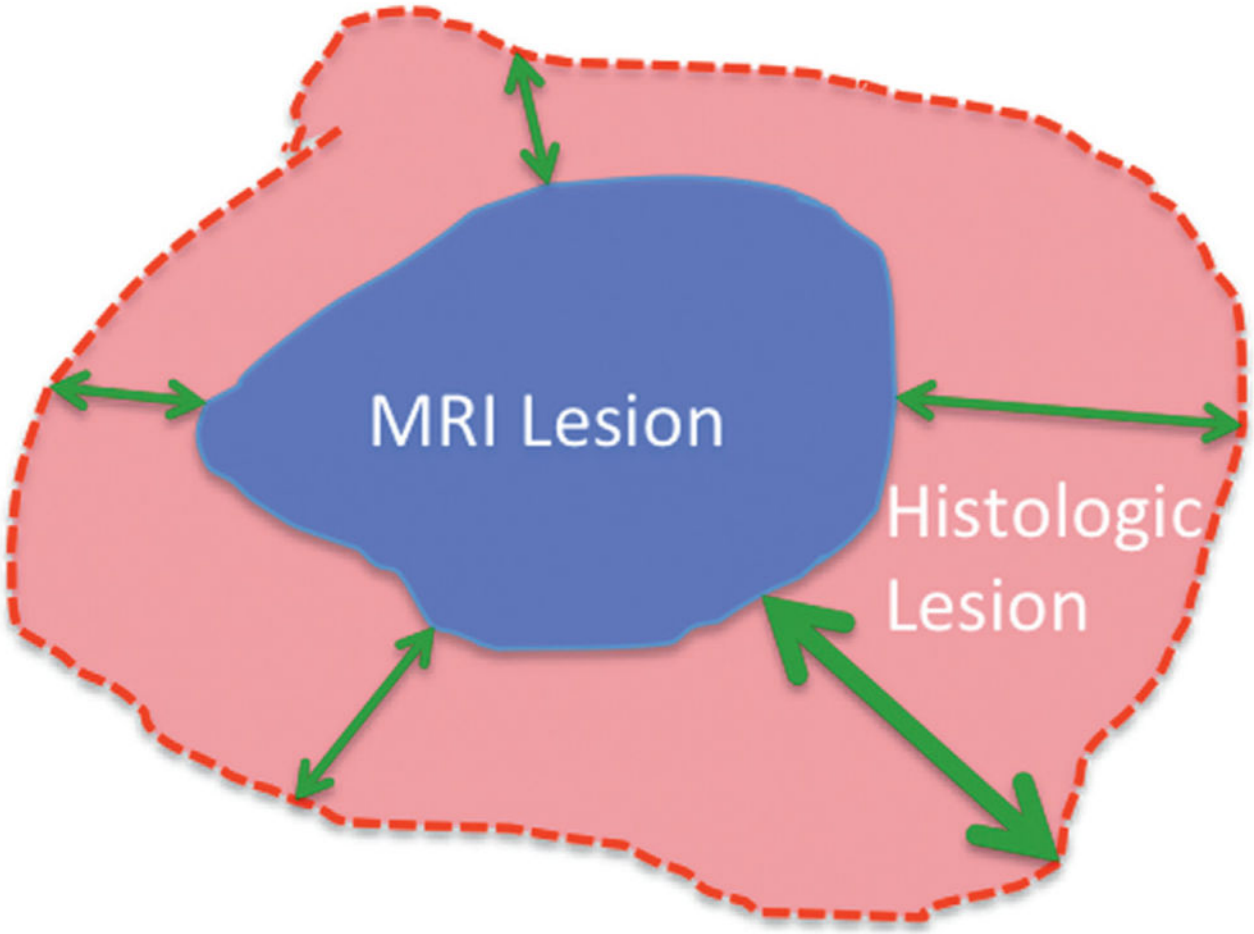

Figure 1.
MRI lesion encompassed by histological lesion. Black outline indicates histological boundary. Small 2-headed arrows indicate HD. Large 2-headed arrows indicate Hausdorff Max.

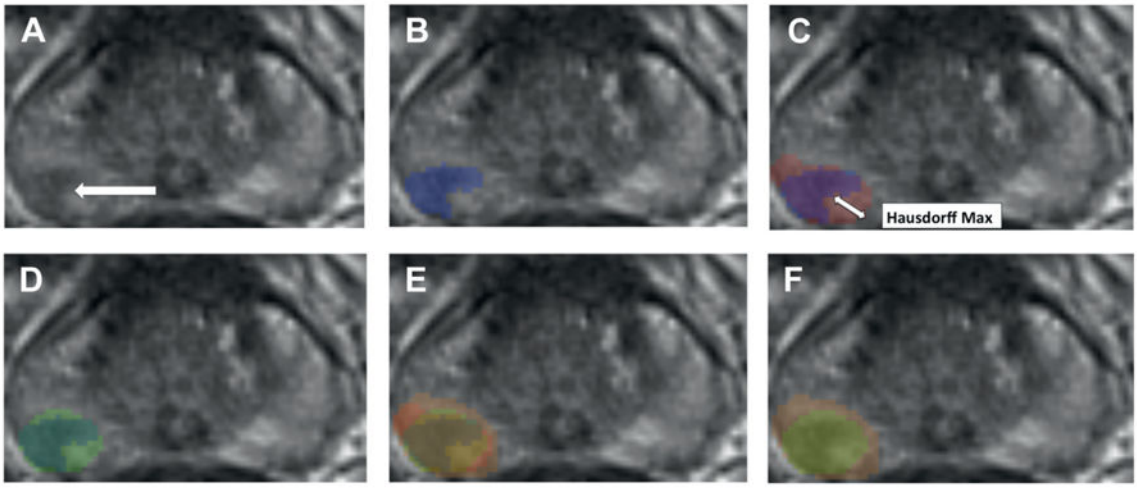

Figure 2.

Focal treatment simulations using theoretical cylinders to define treatment zone. *A*, axial T2WI of prostate shows right posterolateral lesion corresponding to dominant tumor on radical prostatectomy (arrow). *B*, MRI lesion boundaries (blue overlay). *C*, MRI lesion (blue overlay) superimposed on histological lesion (red overlay). *D*, MRI lesion (inner overlay) encompassed by cylinder estimating MRI based treatment zone (outer overlay). *E*, superimposition of MRI lesion (inner overlay), histological lesion (middle overlay) and cylinder estimating treatment zone to achieve complete histological destruction (outer overlay). *F*, superimposition of MRI based (inner overlay) and histological based (outer overlay) treatment cylinders

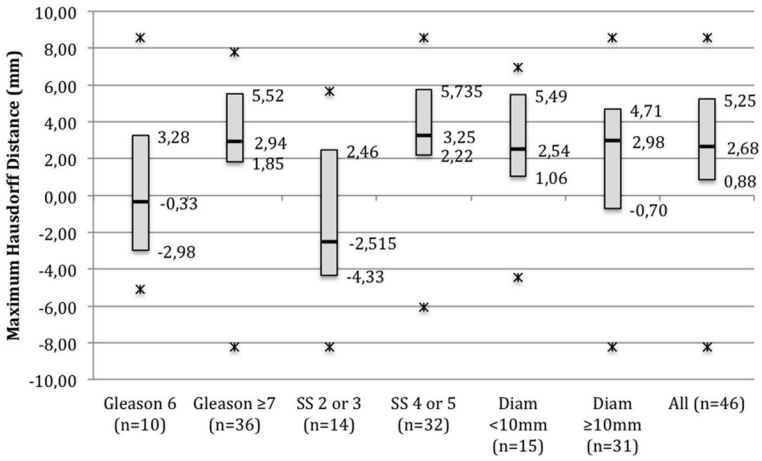

Figure 3.

Maximum HD between MRI and registered histology stratified by tumor characteristics. *Diam*, lesion diameter.

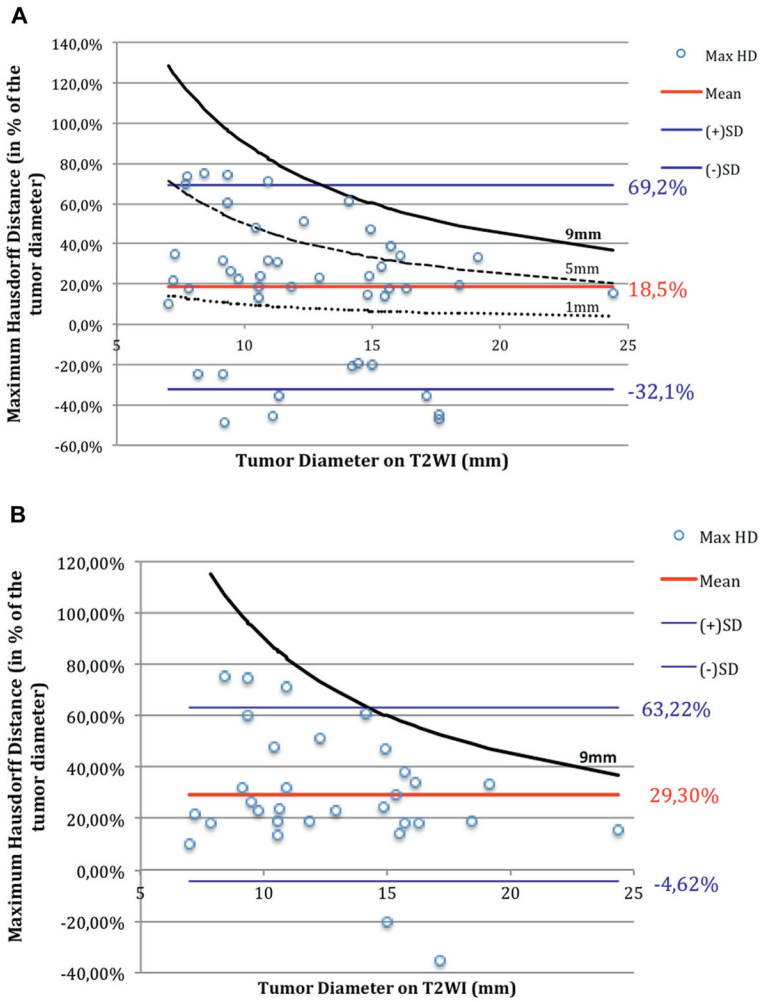

Figure 4.

Maximum HD expressed as percent of MRI tumor diameter on T2WI. All data points fall within 9 mm curve. Each point represents 1 patient. Horizontal lines represent mean ± 95% CI of maximum HD. *A*, in all 46 lesions. Curves represent hypothetical treatment margins around lesion with given MRI diameter when applying 9, 5 and 1 mm treatment margins in cohort. *B*, in 32 lesions with high MRI SS of 4 or 5. Curve represents hypothetical treatment margins around lesion with given MRI diameter when applying 9 mm treatment margins in subset.

Table 1

Characteristics of 33 patients and 46 lesions

	Mean ± SD/Median (range)
Age	60.7 ± 5.4/62 (48–77)
PSA (ng/ml)	6.4 ± 3.4/4.8 (0.3–19.5)
Prostate vol (cc):	
Registered histology	46.6 ± 16.3/42.0 (18.0–99.8)
T2WI	46.9 ± 16.2/40.1 (20.9–106.0)
GS	–/7 (6–9)
MRI SS	–/4 (2–5)
Tumor vol (cc):	
T2WI	0.7 ± 0.5/0.4 (0.1–3.2)
Registered histology	1.1 ± 0.8/0.7 (0.1–4.5)
Largest diameter (mm):	
T2WI	12.5 ± 3.3/11.3 (7.0–24.4)
Registered histology	14.9 ± 5.1/13.0 (4.0–38.3)

Table 2

HD by tumor characteristics

	No. Tumors	Mean ± SD mm HD (% MRI diameter)	Mean ± SD mm Max HD (% MRI diameter)
All tumors	46	0.5 ± 0.9 (4.7 ± 6.9)	1.9 ± 3.1 (18.5 ± 25.9)
SS:			
High	32	0.9 ± 0.6 (7.5 ± 4.5)	3.5 ± 2.1 (29.3 ± 17.3)
Low	14	−0.4 ± 1.0 (−1.6 ± 9.4)	−1.4 ± 3.8 (−6.1 ± 36.4)
GS:			
7 or Greater	36	0.6 ± 0.8 (5.9 ± 6.1)	2.5 ± 2.8 (23.9 ± 23.6)
6	10	0.1 ± 1.0 (0.2 ± 8.3)	0.2 ± 3.8 (−0.6 ± 31.2)
Diameter (mm):			
Less than 10	15	0.6 ± 0.6 (7.3 ± 7.5)	2.3 ± 2.6 (28.1 ± 29.7)
10 or Greater	31	0.4 ± 0.9 (3.4 ± 6.7)	1.8 ± 3.5 (13.9 ± 24.5)

Table 3

Focal treatment simulation to define treatment zone

	Mean MCyl	Mean HCyl
Cylinder diameter (mm)	12.2	16.2
Cylinder vol cc (% prostate vol)	2.38 (5.3)	4.32 (10)
Missed cc vol (%)	0.16 (14.8)	0
Treated benign vol (cc)	1.42	3.14